RSC Advances

PAPER

View Article Online
View Journal | View Issue

Cite this: *RSC Adv.*, 2025, **15**, 6668

Lead ferrite-based heterogeneous photocatalysis: a green approach for rhodamine 6G dye remediation

Bibi Sara,[a] Jameel Ahmed Baig, *[ab] Imam Bakhsh Solangi,[e] Khalil Akhtar,[a] Saima Perveen, [ac] Sajjad Hussain, [d] Fahad Abbasi[e] and Shakoor Ahmed Solangi[a]

Improper dye disposal pollutes the environment and endangers living species, underlining the need for more effective pollution detection systems. Therefore, the current study is focused on developing reliable methods for monitoring and controlling dye release in water using lead ferrite nanoparticles ($PbFe_{12}O_{19}$-NPs) as the most efficient iron-based material. In the current study, $PbFe_{12}O_{19}$-NPs were synthesized by a sol–gel method and characterized by advanced analytical techniques. The obtained finding revealed that the $PbFe_{12}O_{19}$-NPs possess a hexagonal structure with a negative surface charged smooth surface. They have an average particle size of 13.8 nm. The photocatalytic activity of $PbFe_{12}O_{19}$-NPs for the degradation of rhodamine 6G (RG) dye was evaluated under optimized conditions using UV-visible spectroscopy. The $PbFe_{12}O_{19}$-NPs-based developed method showed a degradation efficiency greater than 95% with LOD and LOQ of 0.0043 and 0.014 mg L^{-1}, respectively. Moreover, the $PbFe_{12}O_{19}$-NPs as nano-catalysts showed active reusability and ease of separability due to their magnetic nature. The $PbFe_{12}O_{19}$-NP-based developed method was applied to real water samples and the RG degradation was found to be greater than 90% with an RSD of less than 3.0%.

Received 29th December 2024
Accepted 31st January 2025

DOI: 10.1039/d4ra09072a

rsc.li/rsc-advances

1 Introduction

The rapid growth of the textile industry has significantly contributed to water pollution due to the excessive use of synthetic dyes.[1] Because of the overuse of synthetic dyes, the explosive rise in the textile industry has greatly increased water contamination.[2–5] An estimated 7×10^5 tons of dyes undergo production each year, of which 10–15% are released as effluents.[6] These effluents include toxic organic pigments that are poisonous to aquatic life, frequently non-biodegradable, and carcinogenic.[7–11] Commonly used dyes including Eriochrome Black-T, Methylene Blue, and rhodamine B can have a negative environmental impact even at low quantities (<1 mg L^{-1}) in water bodies.[12–14]

The wastewater treatment techniques, such as adsorption, filtration, and biological degradation, have some drawbacks such as high costs, generation of secondary waste, and insufficient dye degradation.[15] However, the photocatalysis process has been the most efficient, and affordable green solution for dye degradation in recent years.[16] The current studies have observed a significant rise in interest in nanomaterials, particularly metal oxide-based nanoparticles due to their unique properties like large surface area, high stability, and efficient photocatalytic activity.[17,18] Among metal oxides, ferrite-based nanomaterials have shown outstanding potential for environmental remediation.[19,20] There have been several studies on iron-based photocatalysts, and structural changes can significantly impact their catalytic effectiveness.[17–20]

The distinctive family of hexagonal ferrites known as lead hexaferrite ($PbFe_{12}O_{19}$) is well-suited for photocatalytic applications due to its unique magnetic and optical characteristics. The modification of Fe-based catalysts to improve photocatalytic efficiency is still being researched, despite much work on ferrite nanoparticles.[21–24]

In this study, $PbFe_{12}O_{19}$ nanoparticles were synthesized *via* the sol–gel method and characterized using UV-visible spectroscopy, X-ray diffraction (XRD), scanning electron microscopy (SEM), zeta potential (ZP), zeta sizer (ZS), and vibrating sample magnetometry (VSM). The photocatalytic activity of the synthesized $PbFe_{12}O_{19}$ nanoparticles in degrading rhodamine G (RG) dye under exposure to sunlight was assessed. This work seeks to contribute to the development of effective and environmentally acceptable photocatalysts for wastewater treatment by filling the gap in the current ferrite-based nanomaterials and improving their practical application.

[a]*Centre of Excellence in Analytical Chemistry, University of Sindh, Jamshoro 76080, Pakistan. E-mail: jameel.baig@usindh.edu.pk*

[b]*Department of Chemistry, College of Science, Imam Mohammad Ibn Saud Islamic University (IMSIU), P. O. Box 90950, Riyadh 11623, Saudi Arabia*

[c]*Pamukkale University, Faculty of Science, Chemistry Department, Pamukkale, Denizli, Turkey*

[d]*Centre of Excellence in Solid State Physics, University of the Punjab, Lahore, 05422, Pakistan*

[e]*Dr M. A. Kazi Institute of Chemistry, University of Sindh, Jamshoro 76080, Pakistan*

2 Experimental

2.1 Chemicals

Iron nitrate [$Fe(NO_3)_3 \cdot 9H_2O$], lead nitrate $Pb(NO_3)_2$, citric acid ($C_6H_8O_7$), ammonium hydroxide (NH_4OH), rhodamine 6G (RG; $C_{28}H_{31}N_2O_3Cl$), sodium hydroxide (NaOH), and hydrochloric acid (HCl) were obtained from Fluka (Bush, Switzerland). The Centre of Excellence in Analytical Chemistry, located in Jamshoro, Pakistan, provided the deionized (DI) water.

2.2 Synthesis of $PbFe_{12}O_{19}$-NPs by sol–gel method

$PbFe_{12}O_{19}$-NPs were synthesized by a sol–gel method. Stoichiometric amounts of $Fe(NO_3)_3 \cdot 9H_2O$ and $Pb(NO_3)_2$ were mixed in deionized water in 1 : 2 molar concentrations with continuous stirring with the addition of citric acid (2 M) to prevent aggregation (eqn (1)). The pH was maintained at 7 with NH_4OH and promoted hydrolysis and condensation of Fe^{3+} and Pb^{2+} ions (eqn (2)). The resulting mixture was slowly evaporated at 80 °C until a gel was formed. The gel was further heated in an electric oven to remove organic residues and produced Fe_2O_3 and PbO (eqn (3)). The resulting product was calcined in the furnace in an air atmosphere at 900 °C for 3 h to form $PbFe_{12}O_{19}$ nanoparticles (eqn (4)).[25]

$$Fe(NO_3)_3 \cdot 9H_2O + Pb(NO_3)_2 \rightarrow Fe^{3+} + Pb^{2+} + 5NO_3^- + 9H_2O \quad (1)$$

$$Fe^{3+} + Pb^{2+} + NH_4OH \rightarrow Fe(OH)_3 + Pb(OH)_2 \quad (2)$$

$$Fe(OH)_3 + Pb(OH)_2 \rightarrow Fe_2O_3 + PbO + H_2O \quad (3)$$

$$PbO + Fe_2O_3 \rightarrow PbFe_{12}O_{19} \quad (4)$$

2.3 Instrumentation

The pH meter (Eutech, Malaysia) was employed to maintain the pH of the solutions. The XRD and SEM analyses were accomplished by D-8 Bruker and JSM-6380 JEOL instruments to determine the average particle size and surface morphology of the $PbFe_{12}O_{19}$ nanoparticles. The zeta potential and zeta size were studied by a zeta potential analyzer (ELSZ-2000). The nitrogen absorption and desorption of samples were performed at liquid nitrogen temperature (78 K) and gas saturation vapour tension was measured by the Brunauer–Emmett–Teller (BET) surface area analyzer of Quantachrome (Boynton Beach, Florida, USA). The UV-visible spectrophotometer (UV-2600, Shimadzu, Japan) was employed to investigate the band gap of $PbFe_{12}O_{19}$ nanoparticles and to evaluate the catalytic activity of RG dye.

2.4 Photocatalytic analysis

The photocatalytic degradation of RG was performed at room temperature in a designed photo reactor using sunlight with stirring (450 rpm) for photoreaction. The concentration of $PbFe_{12}O_{19}$-NPs (used as a photocatalyst) was studied ranging from 1 to 5 mg in 20 mL of pollutant (RG) with a concentration range of 5–20 mg L^{-1}. The estimated solar irradiance during the experimental period was ranging from 600 to 900 W m^{-2} (regional meteorological data). The initial absorbance was recorded before equilibrium and the final absorbance was recorded after achieving photodegradation equilibrium at 527 nm.[26–28] The sunlight was applied to start the photoreaction with continuous stirring for 20–80 min. After the completion of the reaction, an aliquot of 5 mL was drawn to check the degradation efficiency on the UV-visible spectrophotometer. The schematic diagram of photocatalytic analysis is shown in Fig. 1. The synthesized $PbFe_{12}O_{19}$ nanocatalyst was recycled 12 times to check the efficiency after every experiment. The experiments were performed with repeated washing using water and ethanol.[29] The photodegradation efficiency (%) of RG was determined by the following equation (eqn (5)):

$$\%D = 1 - \frac{C_f}{C_i} \times 100 \quad (5)$$

Where C_i and C_f (mg L^{-1}) represent the initial and final concentrations of RG at 40 min respectively.

2.5 Sampling

The industrial wastewater samples ($n = 5$) were gathered from different sites of the Jamshoro industrial area close to the discharge points. The collected water samples were filtered with Whatman no. 1 filter paper and stored in glass bottles (soaked in 10% HNO_3 and washed with DI water) at 4 °C.

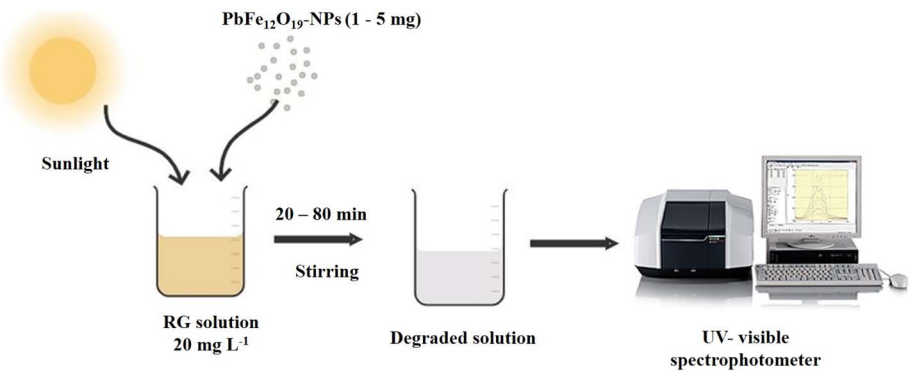

Fig. 1 Schematic diagram of photocatalytic degradation of RG using $PbFe_{12}O_{19}$.

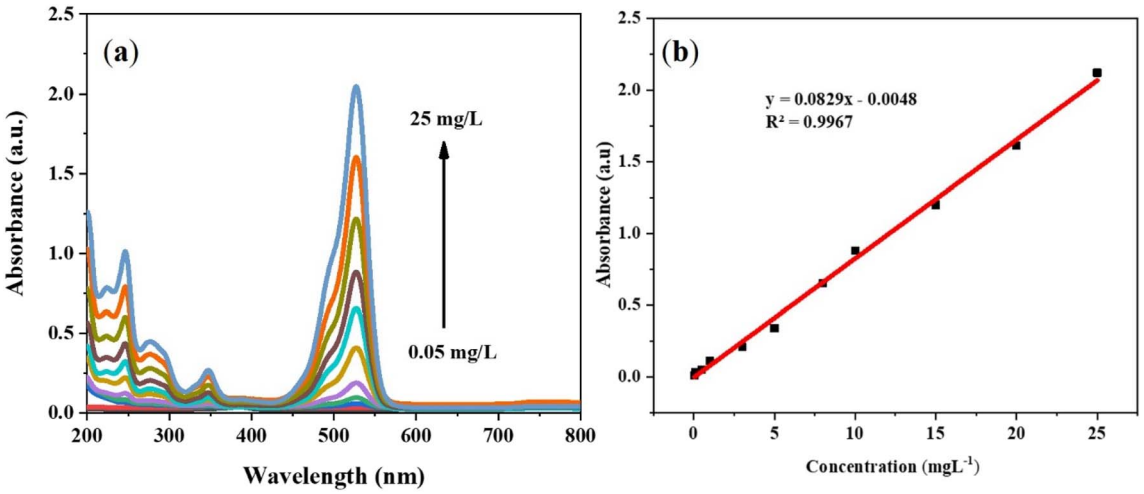

Fig. 2 (a) Calibration curve of RG at different concentrations ranging from 0.05 to 25 mg L^{-1} and (b) the linear relationship between absorbance and concentration.

2.6 UV-visible spectroscopy analysis of RG

The quantitative analysis of RG was conducted by UV-visible spectroscopy technique. The experiments were carried out in DI water. The λ_{max} (wavelength maximum) of RG was found at 527 nm due to π–π^* transitions in their aromatic rings.[30,31] The calibration was drawn by increasing RG concentrations from 0.05 to 25 mg L^{-1} (Fig. 2(a)). Good linearity was observed between the absorbance and varying concentrations of RG with the coefficient of determination (R^2) of 0.9967 (Fig. 2(b)). The limit of detection (LOD) and limit of quantification (LOQ) was found 0.0043 and 0.0145 mg L^{-1}, respectively.

3 Results and discussion

3.1 Characterization of $PbFe_{12}O_{19}$ nanoparticles

The band gap of synthesized $PbFe_{12}O_{19}$-NPs was studied using the UV-visible spectroscopy technique. The absorption band at 355 nm was observed in the obtained spectrum of synthesized $PbFe_{12}O_{19}$-NPs (Fig. 3(a)), confirming particle formation. The band gap of $PbFe_{12}O_{19}$-NPs was calculated by the following equation (eqn (6)).

$$E_g = \frac{1240}{\lambda} \times 100 \quad (6)$$

where E_g is the band gap energy in electron volts (eV), 1240 represents the constant (product of Planck's constant h and speed of light c in eV nm) and λ is the wavelength of the absorption gap in nanometers (nm). By applying this equation, the band gap was found 3.49 eV indicating that the $PbFe_{12}O_{19}$-NPs have potential optical activity and can be applied as photocatalysts for the degradation of RG.[32]

The XRD technique was applied to study the structure, size and degree of crystallinity of $PbFe_{12}O_{19}$-NPs. Fig. 3(b) shows the XRD patterns of $PbFe_{12}O_{19}$-NPs in the range of 20–80°. The diffraction peak pattern at 2θ matched with the hexagonal phase (JCPDS no. 31-0686).[33] The absence of extraneous peaks in the XRD patterns confirmed the successful removal of all unreacted materials and impurities. The average crystallite size of $PbFe_{12}O_{19}$-NPs was assessed using the Debye–Scherrer equation as reported in literature.[34] The average crystallite size of $PbFe_{12}O_{19}$-NPs was found 13.8 nm.

The SEM image of synthesized $PbFe_{12}O_{19}$-NPs showed hexagonal flake shape with smooth surface as shown in Fig. 3(c). Further, the surface of the particles is smooth and the particles are uniformly distributed.[35]

The ZP of synthesized $PbFe_{12}O_{19}$-NPs was investigated and the average ZP of synthesized $PbFe_{12}O_{19}$-NPs was found −31.2 mV which confirmed its stability (Fig. 3(d)).[36] The zeta size of $PbFe_{12}O_{19}$-NPs was also studied (Fig. 3(d)) and the zeta size was found within the nanometer range with an average size of 35.7 nm.[36]

The BET technique was employed to study the specific surface area, pore size and pore volume of synthesized $PbFe_{12}O_{19}$-NPs.[32] The average surface area of synthesized $PbFe_{12}O_{19}$-NPs was found 158.3 m^2 g^{-1} which is very effective for degradation applications. Further, the average pore size and pore volume of $PbFe_{12}O_{19}$-NPs were found 15.94 nm and 45.71 cm^3 g^{-1} respectively. As the average pore size was calculated at 15.94 nm, so the synthesized $PbFe_{12}O_{19}$-NPs are mesoporous (materials having pore sized 2–50 nm) in nature.[37]

3.2 Photocatalyst oxidation mechanism

The applications and outstanding properties of $PbFe_{12}O_{19}$-NPs are due to the excitation of its electrons by absorption of sunlight resulting in the production of the electron–hole (e^-–h^+) pair. This pair contains high oxidizing-reducing potentials that make them able to initiate the first series of chain reactions.[38] Once the $PbFe_{12}O_{19}$-NPs interact with UV light ($\lambda \leq 355$ nm) which is equivalent to or greater than the band gap (3.49 eV), valence band (VB) electrons are excited towards the conduction band and form a positive hole (h^+) in the VB (eqn (7)).

$$PbFe_{12}O_{19} + h\nu \rightarrow e^- + h^+ \quad (7)$$

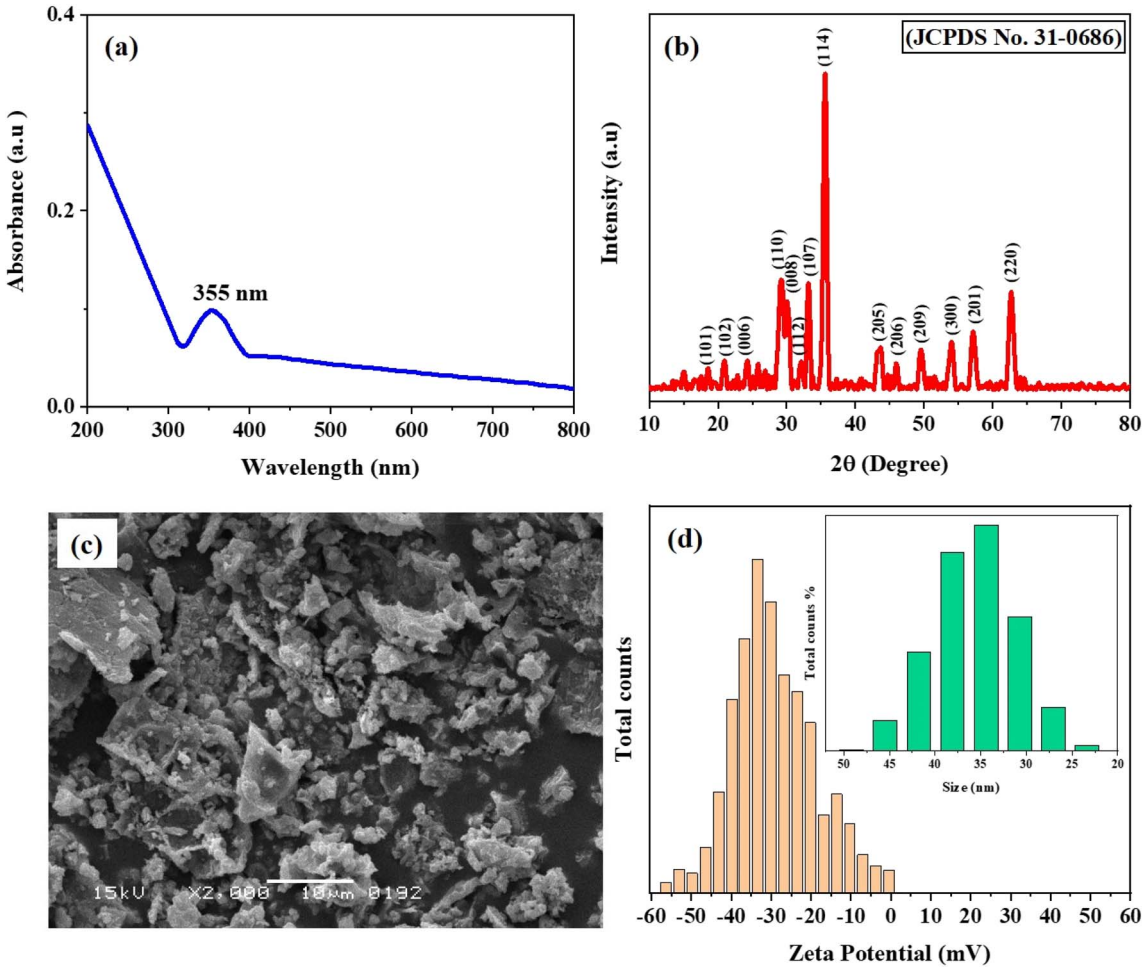

Fig. 3 (a) UV-visible spectrum, (b) XRD spectrum, (c) SEM image, and (d) zeta potential along with zeta size analysis of synthesized $PbFe_{12}O_{19}$ nanoparticles.

The excited electrons (e^-) in the conduction band and the holes (h^+) in the valence band can participate in reduction and oxidation reactions.[39]

The excited electrons (e^-) in the conduction band can reduce adsorbed oxygen (O_2) molecules, forming superoxide radicals ($O_2^{\bullet -}$) (eqn (8)).[40]

$$e^- + O_2 \rightarrow O_2^{\bullet -} \quad (8)$$

The holes (h^+) in the valence band can react with water molecules (H_2O) or hydroxide ions (OH^-) to generate highly reactive hydroxyl radicals ($^{\bullet}OH$) (eqn (9) and (10)).[41]

$$h^+ + H_2O \rightarrow {}^{\bullet}OH + H^+ \quad (9)$$

$$h^+ + OH^- \rightarrow {}^{\bullet}OH \quad (10)$$

The generated reactive oxygen species such as hydroxyl radicals ($^{\bullet}OH$) and superoxide radicals ($O_2^{\bullet -}$) play a crucial role in the degradation of RG (eqn (11)–(13)).[42]

$$RG + {}^{\bullet}OH \rightarrow \text{Degradation product} \quad (11)$$

$$RG + h^+ \rightarrow \text{Oxidation product} \quad (12)$$

$$RG + e^- \rightarrow \text{Reduction product} \quad (13)$$

The RG molecules are attacked by these reactive radicals, which cause them to fragment into smaller, less hazardous pieces, which eventually result in entire mineralization into CO_2 and H_2O.

3.3 Optimization study for the degradation of RG using $PbFe_{12}O_{19}$-NPs

Various factors that affect the rate of photocatalysis may include light source, the initial concentration of RG, catalyst dose, pH, and irradiation time.[43] Therefore, in the present study, these factors were investigated under different operating parameters as discussed below.

Solar lights and artificial lights have been used in dye photodegradation, but mostly artificial light sources can be used to maintain stable intensities away from clouding and other environmental factors.[44] The intensity and wavelength of UV light greatly affect aqueous medium photodegradation. Sunlight irradiation is an alternative and economical light

source due to its abundance, availability and non-hazardous nature.[45] Sunlight consists of 5% UV light (200–400 nm), 43% visible light (400–800 nm) and 52% IR (>52%). Visible light has lower photon energy than UV light. Therefore the experiments were conducted under various conditions including dark, tungsten UV light, and sunlight and excellent results were obtained in sunlight. Fig. 4(a) shows the photodegradation efficiency of 3.0 mg $PbFe_{12}O_{19}$-NPs towards 10 mg L^{-1} RG in different conditions for 40 min. The results indicate that the maximum % degradation was found with sunlight.

Research has shown that the initial degradation rate of RG solution is directly related to photocatalyst concentration. It has also been observed that there is a specific concentration range of photocatalyst for the photocatalyst degradation of each particular pollutant. At the same time, it is considerable that a larger amount of the designated portion can reduce the rate of photocatalyst activity.[46] The main reason behind this fact is that by increasing the amount of photocatalyst, an increase will be caused in the number of active locations that exist on the molecular levels and results in enlarging the number of hydroxyl and superoxide radicals. When the photocatalyst concentration is higher than the optimal amount, a decrease in the rate of photocatalyst degradation is induced, which is related to the light blockage that is created by the raised mass of particles in the suspension.[47] In addition, increasing the concentration of photocatalysts beyond the optimum amount could result in the coagulation of catalyst nanoparticles; therefore, there would be less surface area and consequently less photon absorption, which reduced the rate of photocatalyst degradation. The obtained results of RG degradation compared to various concentrations for sunlight irradiation in 20 min are illustrated in Fig. 4(b) indicating that the maximum degradation efficiency was found at 10 mg L^{-1}.

The degradation of RG was investigated by varying the dosage of photocatalyst ($PbFe_{12}O_{19}$-NPs) ranging from 1.0–5.0 mg. The obtained results of RG degradation at different concentrations of photocatalyst $PbFe_{12}O_{19}$-NPs under sun light irradiation for 40 min are illustrated in Fig. 4(c).

One of the effective factors in the photocatalyst degradation of RG by $PbFe_{12}O_{19}$-NPs in aqueous solutions is known to be the pH. It is a complicated procedure to determine the influence of pH on the efficiency of the optical degradation process of dye materials since it could cause multiple effects on photocatalysis. Moreover, pH can affect the ionization level of

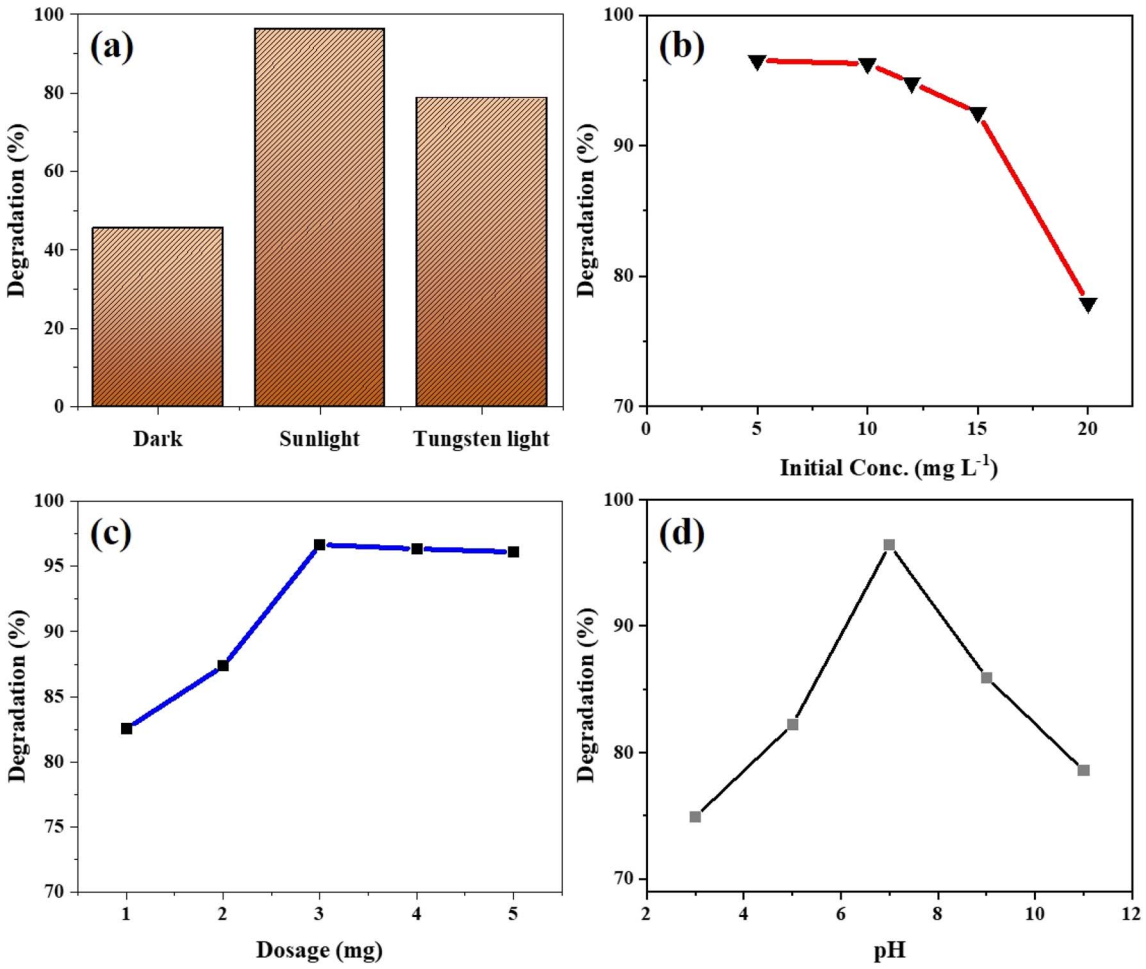

Fig. 4 (a) Effect of irradiation and (b) RG initial concentration, (c) catalyst dose and (d) pH on the degradation efficiency of $PbFe_{12}O_{19}$-NPs towards RG.

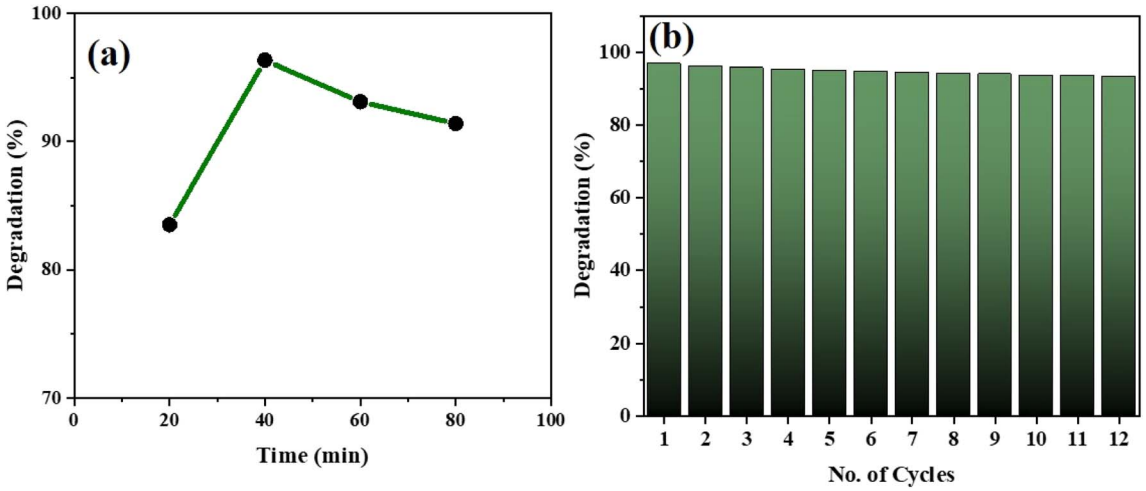

Fig. 5 (a) Contact time and (b) reusability of $PbFe_{12}O_{19}$-NPs over the degradation efficiency towards RG.

photocatalysts, and the nature of reactive dyes. Therefore, it could be stated that the variations of pH have an impact on the absorption of dye molecules, which stands as a crucial stage in the photocatalyst oxidation process.[48] On the other hand, hydroxyl radicals have been observed to be composed of the reaction between hydroxide ions and positive holes. Positive holes are recognized as vital oxidizing species that exist in the lower pH, whereas hydroxyl radicals are the dominant species in neutral or higher pH.[49] In base solutions, the hydroxide ions that are positioned on the surface of $PbFe_{12}O_{19}$-NPs are oxidized, while the hydroxyl radicals are produced through a more natural procedure and consequently, increase the efficiency of the photocatalyst process. There are negative charges between the photocatalyst level and hydroxide anions within the base solutions, which can prevent the production of hydroxyl radicals and therefore, reduce the efficiency of the photochemical process.[50] The performed studies have indicated that $PbFe_{12}O_{19}$-NPs contain a tendency to agglomerate in acidic conditions while in this case, they have been causing a reduction in the surface area. In general, high pH values can prevent the absorption of anionic dyes that are present on the surface of the photocatalyst and contain a negative charge.[48] At low pH, the induced reduction by conduction electrons seems to have an essential role in the procedure of dye degradation. Therefore, it can be suggested that pH stands as a principal agent in the photocatalyst degradation of textile sewage. The results of RG degradation at different pH from 3–11 of photocatalyst $PbFe_{12}O_{19}$-NPs under sunlight irradiation for 40 min are demonstrated in Fig. 4(d).

Time exposure to sunlight is one of the foremost factors in determining the photodegradation capacity of photocatalysts toward RG degradation.[51] It is reported that as irradiation time for photocatalytic reaction increases photodegradation and decolorization of dye increases, which can be attributed to the formation of $^{\bullet}OH$ and $^{\bullet}O_2^-$ with increasing irradiation reaction time.[52] Initially, the degradation rate is faster and slows down upon increasing the irradiation time. 5 displays the outcome of sunlight irradiation time on the photocatalysis of RG. It was found that percent degradation increased with increasing irradiation time. The $PbFe_{12}O_{19}$-NPs degraded 95.5 RG, respectively under sunlight irradiation within 40 min. The percent degradation was progressively increased by increasing the time duration and intensity of light are illustrated in Fig. 5(a).

3.4 Kinetic study

Since photocatalysis is a surface phenomenon the adsorption of dyes onto the surface of the photocatalyst is a crucial step to enhance the photodegradation efficiency.[32] To describe the kinetics of solid/liquid systems, usually, pseudo-kinetic models like pseudo-first-order and pseudo-second-order kinetics are employed.[53] So, the experimental data for the photodegradation of RG dye were fitted to pseudo-first-order and pseudo-second-order kinetic equations to find the appropriate model which represents the kinetics of degradation. In a pseudo-first-order reaction, a straight-line graph is obtained by plotting the logarithm of the ratio of the initial concentration of RG dye to their concentration after photocatalytic degradation ($\log(q_e - q_t)$) against the irradiation time.

The straight-line equation of pseudo-first-order reaction kinetics is given in eqn (14). The slope of the plot represents the first-order rate constant k_1. The regression coefficients for pseudo-first-order reaction kinetics were found 0.96 for RG, respectively.

$$\log(q_e - q_t) = \log q_e - k_1 t \quad (14)$$

Where q_t and q_e (mg g^{-1}) are the amount of dye removed (degradation capacity) at time t and at equilibrium, respectively,

Table 1 Kinetics parameters study for the degradation of RG by $PbFe_{12}O_{19}$-NPs under sunlight

	Regression equation	q_e	k	R^2
Pseudo 1st order	$y = 0.0056x + 0.3723$	2.69	0.0130	0.7538
Pseudo 2nd order	$y = 0.0171x - 0.0436$	22.9	0.0171	0.9991

Table 2 The comparative study of $PbFe_{12}O_{19}$-NPs-based degradation of RG with reported studies

Catalyst	Light	Time (min)	Removal%	Reference
5-wt%CuO NPs/ZIF-8	UV-visible	105	96	58
CaMn3O6	Visible	240	83.1	59
TiO_2	Visible	240	64	60
ZnO/Zn film	UV	30	34	61
$PbFe_{12}O_{19}$-NPs	Sunlight	40	>95	Current study

and k_1 (min^{-1}) represents the rate constant of the pseudo 1st order model.

The degradation of RG on the surface of $PbFe_{12}O_{19}$-NPs was also analyzed using the pseudo 2nd order kinetic. The equation for the pseudo 2nd order reaction is provided in equation eqn (15).

$$t/q_e = 1/k_2{q_e}^2 + t/q_e \quad (15)$$

Where q_t and q_e are the same as described above and k_2 (g mg^{-1} min^{-1}) is the rate constant of the pseudo 2nd order model.

The co-efficient of determination was found 0.9991 RG for pseudo-second-order chemical reaction kinetics as described. The R^2 values of pseudo 2nd order kinetics are closer to unity for RG dye. Therefore, the photocatalytic degradation reaction of RG by $PbFe_{12}O_{19}$-NPs belongs to pseudo 2nd order kinetics. So, the reaction mechanism is found to be chemically rate-controlling.[53,54] The kinetics parameters for the degradation of RG by $PbFe_{12}O_{19}$-NPs is given in Table 1.

3.5 Reusability

The $PbFe_{12}O_{19}$-NPs nanocatalyst demonstrated effective reusability in successive catalytic experiments, with repeated washing using water and ethanol.[29] The photocatalyst was tested in RG degradation efficiency from 93.3% to 96.8% (Fig. 5(b)). This minor decline in performance (less than 10%) underscores the strong reusability of the catalyst. The reduction in photocatalytic activity may be attributed to: (a) loss of catalyst during the recovery process (washing and drying), which could lead to reduced dosage and subsequently lower surface activity in subsequent cycles;[55] and (b) changes in the photocatalyst properties, such as agglomeration (leading to fewer active sites and lower surface area) and fouling, over repeated cycles.[56] Furthermore, the reduction in adsorption capacity, due to pore blockage by dye molecules (RG) and their intermediates, may contribute to the decline in catalytic activity after multiple cycles.[57] Despite this slight reduction, the $PbFe_{12}O_{19}$-NPs photocatalyst retains significant reusability, making it a promising candidate for long-term industrial applications.

Table 3 Application of the developed method to real water samples

Samples	Initial conc. (mg L^{-1})	Final conc. (mg L^{-1})	Degradation (%)	RSD (%)
01	8.05	0.54	93.3	2.54
02	5.42	0.23	95.7	2.43
03	4.12	0.13	96.8	2.65

3.6 Comparative study and real sample analysis

The analytical performance of $PbFe_{12}O_{19}$-NPs-based degradation of RG was compared with reported studies. Table 2 shows that the degradation of RG is better than that of currently reported studies. Further, to validate the practical applicability of the developed method, it was applied to real samples and the percent degradation was found greater than 90% with a percent relative standard deviation of less than 3. This indicates that the developed method is reliable for the monitoring of dyes in water (Table 3).

4 Conclusion

$PbFe_{12}O_{19}$-NPs were successfully synthesized using the sol–gel method, resulting in the soft magnetic material, average size of 13.8 nm with a hexagonal crystal structure and negatively charged surface. The synthesized $PbFe_{12}O_{19}$-NPs were employed as photocatalysts for the degradation of RG under optimized conditions including sunlight source, initial concentration of 10 mg L^{-1}, 3 mg of photocatalyst dosage, pH 7, and 40 min contact time. The $PbFe_{12}O_{19}$-NPs demonstrated outstanding recovery rates (>90%) for the analysis of water samples which confirmed its practical applicability for environmental monitoring. $PbFe_{12}O_{19}$-NPs was found to be highly efficient for the photodegradation of rhodamine 6G dye, with more than 95% removal.

Approval of ethics

The present experimental studies do not involve any animal/human participants.

Data availability

Access to the information that supports the current study will be provided at the official request.

Author contributions

The current study is a result of the visionary work of Dr Jameel Ahmed Baig, along with Dr Imam Bakhsh Solangi, whose role was in supervision, project management, review, and editing. A committed MPhil. student, Ms Sara Abbasi, was instrumental in the original draft's creation, formal analysis, data curation, and

methodology. The PhD candidates Khalil Akhtar, Saima Perveen, Sajjad Hussain, Fahad Abbasi and Shakoor Ahmed Solangi expertly managed the technical parts, which included software use, research, and visualization.

Conflicts of interest

The authors state that none of the work presented in this study may have been influenced by any known conflicting financial interests or personal ties.

Acknowledgements

The University of Sindh, Jamshoro's National Centre of Excellence in Analytical Chemistry (NCEAC) has been recognized for providing well-equipped laboratory facilities for research projects. The authors acknowledge and extend their appreciation to the Researchers Supporting NRPU Project No.14503 of HEC Islamabad, partially support by Türkiye Bursları Research Fellowship Program sponsored by the Prime Ministry of Turkey Presidency 2023 and National Centre of Excellence in Analytical Chemistry, University of Sindh, Jamshoro.

References

1 J. T. Spadaro, L. Isabelle and V. Renganathan, Hydroxyl radical mediated degradation of azo dyes: evidence for benzene generation, *Environ. Sci. Technol.*, 1994, **28**(7), 1389–1393.
2 I. K. Konstantinou and T. A. Albanis, TiO2-assisted photocatalytic degradation of azo dyes in aqueous solution: kinetic and mechanistic investigations: a review, *Appl. Catal., B*, 2004, **49**(1), 1–14.
3 F. Deng, L. Min, X. Luo, S. Wu and S. Luo, Visible-light photocatalytic degradation performances and thermal stability due to the synergetic effect of TiO 2 with conductive copolymers of polyaniline and polypyrrole, *Nanoscale*, 2013, **5**(18), 8703–8710.
4 S. Xu, Y. Zhu, L. Jiang and Y. Dan, Visible light induced photocatalytic degradation of methyl orange by polythiophene/TiO 2 composite particles, *Water, Air, Soil Pollut.*, 2010, **213**, 151–159.
5 D. Wang, Y. Wang, X. Li, Q. Luo, J. An and J. Yue, Sunlight photocatalytic activity of polypyrrole–TiO2 nanocomposites prepared by '*in situ*'method, *Catal. Commun.*, 2008, **9**(6), 1162–1166.
6 A. Kumar and G. Pandey, A review on the factors affecting the photocatalytic degradation of hazardous materials, *Mater. Sci. Eng. Int. J.*, 2017, **1**(3), 1–10.
7 S. Sabir, M. Arshad and S. K. Chaudhari, Zinc oxide nanoparticles for revolutionizing agriculture: synthesis and applications, *Sci. World J.*, 2014, **2014**(1), 925494.
8 L. Keith and W. Telliard, ES&T special report: priority pollutants: Ia perspective view, *Environ. Sci. Technol.*, 1979, **13**(4), 416–423.
9 A. M. Idris, M. I. Shinger, D. D. Qin, H. Baballa and X. Lu, An in-situ anion exchange method synthesized of Ag3PO4 functionalized with Fe3O4 and AgI for photocatalytic degradation of methyl orange under visible light irradiation, *Am. J. Nanosci. Nanotechnol.*, 2014, **2**(5), 115–120.
10 W. Zhu, Z. Xia, B. Shi and C. Lü, Water-triggered conversion of Cs4PbBr6@ TiO2 into Cs4PbBr6/CsPbBr3@ TiO2 three-phase heterojunction for enhanced visible-light-driven photocatalytic degradation of organic pollutants, *Mater. Today Chem.*, 2022, **24**, 100880.
11 E. Parvizi, *et al.*, Photocatalytic efficacy of supported tetrazine on MgZnO nanoparticles for the heterogeneous photodegradation of methylene blue and ciprofloxacin, *RSC Adv.*, 2019, **9**(41), 23818–23831.
12 N. Daneshvar, D. Salari and A. Khataee, Photocatalytic degradation of azo dye acid red 14 in water: investigation of the effect of operational parameters, *J. Photochem. Photobiol. Chem.*, 2003, **157**(1), 111–116.
13 S. Ledakowicz and M. Gonera, Optimisation of oxidants dose for combined chemical and biological treatment of textile wastewater, *Water Res.*, 1999, **33**(11), 2511–2516.
14 J. Grzechulska and A. W. Morawski, Photocatalytic decomposition of azo-dye acid black 1 in water over modified titanium dioxide, *Appl. Catal., B*, 2002, **36**(1), 45–51.
15 L. Gnanasekaran, *et al.*, Synthesis and characterization of metal oxides (CeO2, CuO, NiO, Mn3O4, SnO2 and ZnO) nanoparticles as photo catalysts for degradation of textile dyes, *J. Photochem. Photobiol., B*, 2017, **173**, 43–49.
16 N. Hareesha, J. Manjunatha, C. Raril and G. Tigari, Sensitive and selective electrochemical resolution of tyrosine with ascorbic acid through the development of electropolymerized alizarin sodium sulfonate modified carbon nanotube paste electrodes, *ChemistrySelect*, 2019, **4**(15), 4559–4567.
17 M. Manimohan, S. Pugalmani, K. Ravichandran and M. A. Sithique, Synthesis and characterisation of novel Cu (II)-anchored biopolymer complexes as reusable materials for the photocatalytic degradation of methylene blue, *RSC Adv.*, 2020, **10**(31), 18259–18279.
18 R. Chen, Z. Jalili and R. Tayebee, UV-visible light-induced photochemical synthesis of benzimidazoles by coomassie brilliant blue coated on W–ZnO@ NH 2 nanoparticles, *RSC Adv.*, 2021, **11**(27), 16359–16375.
19 S. Rajendrachari, B. K. Swamy, S. Reddy and D. Chaira, Synthesis of silver nanoparticles and their applications, *Anal. Bioanal. Electrochem.*, 2013, **5**(4), 455–466.
20 S. Reddy, B. K. Swamy, S. Aruna, M. Kumar, R. Shashanka and H. Jayadevappa, Preparation of NiO/ZnO hybrid nanoparticles for electrochemical sensing of dopamine and uric acid, *Chem. Senses*, 2012, **2**(1), 1–8.
21 V. U. Pandit, *et al.*, Hierarchical CdS nanostructure by Lawesson's reagent and its enhanced photocatalytic hydrogen production, *RSC Adv.*, 2015, **5**(18), 13715–13721.
22 M. Jarrahi, R. Tayebee, B. Maleki and A. Salimi, One-pot multicomponent green LED photoinduced synthesis of chromeno [4, 3-b] chromenes catalyzed by a new nanophotocatalyst histaminium tetrachlorozincate, *RSC Adv.*, 2021, **11**(32), 19723–19736.

23 R. Tayebee, E. Esmaeili, B. Maleki, A. Khoshniat, M. Chahkandi and N. Mollania, Photodegradation of methylene blue and some emerging pharmaceutical micropollutants with an aqueous suspension of WZnO-NH2@ H3PW12O40 nanocomposite, *J. Mol. Liq.*, 2020, **317**, 113928.

24 V. U. Pandit, S. S. Arbuj, U. P. Mulik and B. B. Kale, Novel functionality of organic 6, 13-pentacenequinone as a photocatalyst for hydrogen production under solar light, *Environ. Sci. Technol.*, 2014, **48**(7), 4178–4183.

25 S. M. Ghahfarokhi, Z. Rostami and I. Kazeminezhad, Fabrication of PbFe12O19 nanoparticles and study of their structural, magnetic and dielectric properties, *J. Magn. Magn. Mater.*, 2016, **399**, 130–142.

26 N. Yudasari, *et al.*, Enhanced photocatalytic degradation of rhodamine 6G (R6G) using ZnO–Ag nanoparticles synthesized by pulsed laser ablation in liquid (PLAL), *J. Alloys Compd.*, 2021, **886**, 161291.

27 Y. Chao, *et al.*, Graphene-like BN@ SiO2 nanocomposites as efficient sorbents for solid-phase extraction of Rhodamine B and Rhodamine 6G from food samples, *Food Chem.*, 2020, **320**, 126666.

28 H. Huang, *et al.*, Noble-Metal-Free High-Entropy Alloy Nanoparticles for Efficient Solar-Driven Photocatalytic CO2 Reduction, *Adv. Mater.*, 2024, 2313209.

29 R. Jasrotia, *et al.*, Photocatalytic dye degradation efficiency and reusability of Cu-substituted Zn-Mg spinel nanoferrites for wastewater remediation, *J. Water Proc. Eng.*, 2022, **48**, 102865.

30 W. Dong, *et al.*, Excellent photocatalytic degradation activities of ordered mesoporous anatase TiO2–SiO2 nanocomposites to various organic contaminants, *J. Hazard Mater.*, 2012, **229**, 307–320.

31 A. R. Gollakota, V. S. Munagapati, S. Gautam, J.-C. Wen and C.-M. Shu, Hydrothermal tuning of morphology of aluminophosphate (AlPO-14) framework for the adsorption of Rhodamine 6G dye, *Adv. Powder Technol.*, 2021, **32**(8), 3002–3015.

32 S. Samejo, *et al.*, Green synthesis of iron oxide nanobiocomposite for the adsorptive removal of heavy metals from the drinking water, *Mater. Chem. Phys.*, 2003, **303**, 127807.

33 F. Ansari and M. Salavati-Niasari, Simple sol-gel auto-combustion synthesis and characterization of lead hexaferrite by utilizing cherry juice as a novel fuel and green capping agent, *Adv. Powder Technol.*, 2016, **27**(5), 2025–2031.

34 D. Kumar, M. Singh, and A. K. Singh, Crystallite size effect on lattice strain and crystal structure of Ba1/4Sr3/4MnO3 layered perovskite manganite, in *AIP Conference Proceedings*, AIP Publishing, 2018, vol. 1953, no. 1.

35 X. Ni, L. Chen, H. Zheng, D. Zhang, Q. Zhao and J. Song, Synthesis of nickel nanocrystallites with hexagonal flake-like morphology from nickel dimethylglyoximate, *Chem. Lett.*, 2004, **33**(12), 1564–1565.

36 J. D. Clogston and A. K. Patri, *"Zeta Potential Measurement"*, pp. 63–70, 2011.

37 K. Pan, *et al.*, Low-temperature solution synthesis and characterization of enhanced titanium dioxide photocatalyst on tailored mesoporous γ-Al2O3 support, *Compos. Commun.*, 2020, **19**, 82–89.

38 Z. Sabouri, A. Akbari, H. A. Hosseini, A. Hashemzadeh and M. Darroudi, Eco-friendly biosynthesis of nickel oxide nanoparticles mediated by okra plant extract and investigation of their photocatalytic, magnetic, cytotoxicity, and antibacterial properties, *J. Cluster Sci.*, 2019, **30**, 1425–1434.

39 W. Sun, L. Xiao and X. Wu, Facile synthesis of NiO nanocubes for photocatalysts and supercapacitor electrodes, *J. Alloys Compd.*, 2019, **772**, 465–471.

40 X. Wan, M. Yuan, S.-l. Tie and S. Lan, Effects of catalyst characters on the photocatalytic activity and process of NiO nanoparticles in the degradation of methylene blue, *Appl. Surf. Sci.*, 2013, **277**, 40–46.

41 A. Mardiroosi, A. R. Mahjoub and H. Fakhri, Efficient visible light photocatalytic activity based on magnetic graphene oxide decorated ZnO/NiO, *J. Mater. Sci.: Mater. Electron.*, 2017, **28**, 11722–11732.

42 A. Akbari, Z. Sabouri, H. A. Hosseini, A. Hashemzadeh, M. Khatami and M. Darroudi, Effect of nickel oxide nanoparticles as a photocatalyst in dyes degradation and evaluation of effective parameters in their removal from aqueous environments, *Inorg. Chem. Commun.*, 2020, **115**, 107867.

43 A. Aziz, *et al.*, Chitosan-zinc sulfide nanoparticles, characterization and their photocatalytic degradation efficiency for azo dyes, *Int. J. Biol. Macromol.*, 2020, **153**, 502–512.

44 C. Lydia and G. A. G. Raj, A review on photodegradation of various dyes using photocatalysts, *Int. J. Adv. Sci. Res. Manag.*, 2019, **4**, 37–42.

45 K. M. Reza, A. Kurny and F. Gulshan, Parameters affecting the photocatalytic degradation of dyes using TiO 2: a review, *Appl. Water Sci.*, 2017, **7**, 1569–1578.

46 F. Soofivand and M. Salavati-Niasari, Step synthesis and photocatalytic activity of NiO/graphene nanocomposite under UV and visible light as an effective photocatalyst, *J. Photochem. Photobiol., A*, 2017, **337**, 44–53.

47 F. Torki and H. Faghihian, Photocatalytic activity of NiS, NiO and coupled NiS–NiO for degradation of pharmaceutical pollutant cephalexin under visible light, *RSC Adv.*, 2017, **7**(86), 54651–54661.

48 K. Hayat, M. Gondal, M. M. Khaled and S. Ahmed, Effect of operational key parameters on photocatalytic degradation of phenol using nano nickel oxide synthesized by sol–gel method, *J. Mol. Catal. A: Chem.*, 2011, **336**(1–2), 64–71.

49 N. K. Nasab, Z. Sabouri, S. Ghazal and M. Darroudi, Green-based synthesis of mixed-phase silver nanoparticles as an effective photocatalyst and investigation of their antibacterial properties, *J. Mol. Struct.*, 2020, **1203**, 127411.

50 S. Senobari and A. Nezamzadeh-Ejhieh, A comprehensive study on the enhanced photocatalytic activity of CuO-NiO nanoparticles: designing the experiments, *J. Mol. Liq.*, 2018, **261**, 208–217.

51 M. Makeswari and P. Saraswathi, Photo catalytic degradation of methylene blue and methyl orange from aqueous solution using solar light onto chitosan bi-metal oxide composite, *SN Appl. Sci.*, 2020, **2**(3), 336.

52 S. Sakthivel, B. Neppolian, M. Shankar, B. Arabindoo, M. Palanichamy and V. Murugesan, Solar photocatalytic degradation of azo dye: comparison of photocatalytic efficiency of ZnO and TiO2, *Sol. Energy Mater. Sol. Cells*, 2003, **77**(1), 65–82.

53 M. Hamza, *et al.*, Catalytic removal of alizarin red using chromium manganese oxide nanorods: degradation and kinetic studies, *Catalysts*, 2020, **10**(10), 1150.

54 M. Hamza, *et al.*, Catalytic removal of alizarin red using chromium manganese oxide nanorods: degradation and kinetic studies, *Catalysts*, 2020, **10**(10), 1150.

55 J. Joo, Y. Ye, D. Kim, J. Lee and S. Jeon, Magnetically recoverable hybrid TiO2 nanocrystal clusters with enhanced photocatalytic activity, *Mater. Lett.*, 2013, **93**, 141–144.

56 S. Moosavi, *et al.*, Methylene blue dye photocatalytic degradation over synthesised Fe3O4/AC/TiO2 nano-catalyst: degradation and reusability studies, *Nanomaterials*, 2020, **10**(12), 2360.

57 M. Kermani, B. Kakavandi, M. Farzadkia, A. Esrafili, S. F. Jokandan and A. Shahsavani, Catalytic ozonation of high concentrations of catechol over TiO2@ Fe3O4 magnetic core-shell nanocatalyst: Optimization, toxicity and degradation pathway studies, *J. Cleaner Prod.*, 2018, **192**, 597–607.

58 A. Chakraborty, D. A. Islam and H. J. Acharya, Facile synthesis of CuO nanoparticles deposited zeolitic imidazolate frameworks (ZIF-8) for efficient photocatalytic dye degradation, *J. Solid State Chem.*, 2019, **269**, 566–574.

59 B. Barrocas, S. Sério and M. J. T. Melo Jorge, Hierarchically grown CaMn3O6 nanorods by RF magnetron sputtering for enhanced visible-light-driven photocatalysis, *J. Phys. Chem. C*, 2014, **118**(41), 24127–24135.

60 R. Atchudan, T. N. J. I. Edison, S. Perumal, D. Karthikeyan and Y. R. Lee, Effective photocatalytic degradation of anthropogenic dyes using graphene oxide grafting titanium dioxide nanoparticles under UV-light irradiation, *J. Photochem. Photobiol., A*, 2017, **333**, 92–104.

61 L. Kaliraj, *et al.*, Synthesis of panos extract mediated ZnO nano-flowers as photocatalyst for industrial dye degradation by UV illumination, *J. Photochem. Photobiol., B*, 2019, **199**, 111588.